


## RESEARCH ARTICLE OPEN ACCESS

# Cortical Actin Depolymerisation in 3D Cell Culture Enhances Extracellular Vesicle Secretion and Therapeutic Effects

Zhen Yang<sup>1,2</sup> | Xiaoke Li<sup>3</sup> | Qiyuan Lin<sup>1,2</sup> | Fanfan Zhou<sup>1,2</sup> | Kaini Liang<sup>4</sup> | Jiao Jiao Li<sup>5</sup> | Yudi Niu<sup>4</sup> | Qingchen Meng<sup>1,2</sup> | Tianyuan Zhao<sup>6</sup> | Hao Li<sup>7</sup> | Du Wang<sup>1,2</sup> | Jianjing Lin<sup>8</sup> | Hui Li<sup>1,2</sup> | Bin Wang<sup>9</sup> | Wei Liu<sup>10</sup> | Yanan Du<sup>4</sup> | Jianhao Lin<sup>1,2</sup> | Dan Xing<sup>1,2</sup> 

<sup>1</sup>Arthritis Clinical and Research Center, Peking University People's Hospital, Beijing, China | <sup>2</sup>Arthritis Institute, Peking University, Beijing, China | <sup>3</sup>Department of Orthopaedics, Shanxi Medical University Second Affiliated Hospital, Taiyuan, China | <sup>4</sup>School of Biomedical Engineering, School of Medicine, Tsinghua-Peking Center for Life Sciences, Tsinghua University, Beijing, China | <sup>5</sup>School of Biomedical Engineering, Faculty of Engineering and IT, University of Technology Sydney, Sydney, Australia | <sup>6</sup>Department of Orthopedics, Peking University Third Hospital, Beijing, China | <sup>7</sup>Institute of Orthopedics, the First Medical Center, Chinese PLA General Hospital, Beijing Key Lab of Regenerative Medicine in Orthopedics, Key Laboratory of Musculoskeletal Trauma & War Injuries PLA, Beijing, China | <sup>8</sup>Department of Sports Medicine and Rehabilitation, Peking University Shenzhen Hospital, Shenzhen, China | <sup>9</sup>Department of Orthopaedic Surgery, The First Affiliated Hospital, Zhejiang University School of Medicine, Hangzhou, China | <sup>10</sup>Beijing CytoNiche Biotechnology Co. Ltd, Beijing, China

**Correspondence:** Wei Liu ([liuwei@cytoniche.com](mailto:liuwei@cytoniche.com)) | Yanan Du ([duyanan@tsinghua.edu.cn](mailto:duyanan@tsinghua.edu.cn)) | Jianhao Lin ([linjianhao@pkuph.edu.cn](mailto:linjianhao@pkuph.edu.cn)) | Dan Xing ([xingdan@bjmu.edu.cn](mailto:xingdan@bjmu.edu.cn))

**Received:** 1 November 2024 | **Revised:** 9 April 2025 | **Accepted:** 19 May 2025

**Funding:** This work was funded by grants from Beijing Natural Science Foundation (L222087), Peking University Clinical Scientist Training Program (BMU2024PYJH015, supported by "the Fundamental Research Funds for the Central Universities"), Natural Science Foundation of China (82272538), and Innovation Fund for Outstanding Doctoral Students of Peking University Health Science Center.

**Keywords:** 3D culture | actin depolymerisation | cortical actin | Rab27A/B | small extracellular vesicles

## ABSTRACT

Three-dimensional (3D) culture systems have been shown to enhance cellular secretion of small extracellular vesicles (sEVs) compared to two-dimensional (2D) culture. However, the molecular mechanisms driving sEV secretion and influencing their potential for disease treatment have not been elucidated. In this study, we discovered the depolymerisation of cortical actin as a new mechanism that leads to increased sEV release, and that in 3D cultured mesenchymal stem cells (MSCs), this process was modulated by the downregulation of integrin- $\alpha 1$  (ITGA1) and subsequent inhibition of the RhoA/cofilin signalling pathway. Interestingly, the knockdown of Rab27A and Rab27B significantly reduced sEV secretion by MSCs to 0.5- and 0.1-fold, respectively. However, there was no difference in expression levels of Rab27A/B between MSCs cultured in 2D and 3D environments. In addition, sEVs derived from 3D cultured MSCs demonstrated enhanced therapeutic function both in vitro and in rat models of osteoarthritis (OA) and wound healing. Collectively, this study illustrates a new mechanism for enhanced secretion of sEVs, involving RhoA/cofilin pathway-dependent cortical actin depolymerisation, which is independent of Rab27A/B. These findings provide novel insights for optimising the yield of stem cell-derived sEVs, as well as their therapeutic efficacy for treating chronic diseases.

Zhen Yang, Xiaoke Li, Qiyuan Lin and Fanfan Zhou contributed equally to this work.

This is an open access article under the terms of the [Creative Commons Attribution-NonCommercial](https://creativecommons.org/licenses/by-nc/4.0/) License, which permits use, distribution and reproduction in any medium, provided the original work is properly cited and is not used for commercial purposes.

© 2025 The Author(s). *Journal of Extracellular Vesicles* published by Wiley Periodicals LLC on behalf of International Society for Extracellular Vesicles.

## 1 | Introduction

Small extracellular vesicles (sEVs) are lipid membrane-enclosed nanoparticles released by almost all cell types, typically ranging from 20 to 200 nm, with critical functions in intercellular communication by transferring various signalling molecules and cellular components such as proteins, lipids, nucleic acids and metabolites (Jeppesen et al. 2019; Welsh et al. 2024). sEVs have been increasingly explored as a safer and more versatile alternative to cell therapy in numerous disease models, since they circumvent the inherent limitations of injecting live cells, such as tumorigenic potential, ethical concerns, immunogenicity and systemic or local toxicity (Zhang and Cheng 2023). However, the popularity of using sEVs as disease therapeutics has been limited by the expansion potential of source cells, particularly if the parent cells have a finite lifespan, introducing difficulties in upscaling EV production from preclinical testing to levels meaningful for clinical application. Recently, 3D cell culture systems such as bioreactors and cell spheroids have emerged as sophisticated platforms for large-scale EV production, providing 3D environments closely mirroring in vivo physiological conditions and mechanical stimuli to enhance cellular responses and EV secretion (Centeno et al. 2018; Mo et al. 2018). For example, recent studies have demonstrated that various 3D culture methods can promote sEV production by 2- to 19.4-fold, which may be related to the activation of secretory pathways that are both dependent and independent of the Endosomal Sorting Complex Required for Transport (ESCRT) machinery, as well as the upregulation of sEV biogenesis markers and glycolysis genes (Yuan et al. 2022; Yan and Wu 2020; Cao et al. 2020; Jeske et al. 2023). However, the downstream mechanisms for regulating sEV secretion are not well understood (Mo et al. 2018; Sart et al. 2014).

sEV secretion is preceded by a series of dynamic processes involving intracellular transport and the plasma membrane. Initially, intraluminal vesicles (ILVs) or the precursors of sEVs are formed within multivesicular bodies (MVBs) by inward budding of the MVB membrane into the lumen. Some of the 'secretory MVBs' are then transported to the plasma membrane, where ultimate fusion with the cell membrane leads to the secretion of ILVs into the extracellular space as sEVs (Matsui et al. 2022). Approximately 60 Rab family small GTPases are involved in intracellular transport pathways by switching between active (GTP-bound) and inactive (GDP-bound) forms, and interacting with effector proteins (Hutagalung and Novick 2011; Zerial and McBride 2001). In particular, Rab27A and Rab27B regulate vesicle transport along the cytoskeleton and microtubules by binding with specific effector proteins, ensuring that vesicles move along the microtubules towards the cell membrane (Alzahofi et al. 2020). Cortical actin forms a dense meshwork adjacent to the plasma membrane and normally acts as a barrier to prevent vesicles from reaching the membrane in resting conditions, while an acute reduction in cortical actin has been shown to facilitate vesicle secretion in many cells (Ritter et al. 2017). However, some research has reported that the formation of a cortical actin framework around exocytosing granules can actually promote the movement of vesicular cargo towards the plasma membrane (Li et al. 2018; Papadopoulos et al. 2015). Thus, cortical actin could play a significant role in regulating sEV secretion, although the exact mechanisms and interactions remain poorly understood.

When subjected to 3D culture conditions, cells undergo significant changes in their structural characteristics and appearance (Kouroupis and Correa 2021). For instance, adherent fibroblastic cells such as mesenchymal stem cells (MSCs) transition from a flat spindle-like morphology to a more rounded appearance, accompanied by a marked reduction in cell volume concurrent with loss of tension in the F-actin cytoskeleton, which is essential for the formation of 3D-spheroids (Cesarz and Tamama 2016). Furthermore, treating cells with Cytochalasin D (cytoD) has been shown to change their vesicle secretion levels (Mo et al. 2018). For cells grown in 3D culture, integrins are pivotal in mediating cell-cell adhesion and influencing cellular responses to spatial cues. The activation of integrin receptors initiates a cascade of intracellular events, with the RhoA pathway emerging as a key player in orchestrating downstream cytoskeletal dynamics (Yu et al. 2020; Lin et al. 2003). These cytoskeletal changes occurring as a result of 3D culture may have a pivotal role in regulating cortical actin depolymerisation and sEV secretion, but the detailed mechanisms have not been investigated.

MSCs have been a popular source of stem cell-derived sEVs aimed at therapeutic applications due to their inherent paracrine functions. Compared to the parent cells, sEVs derived from MSCs have exhibited comparable therapeutic effects in various disease models, including their anti-inflammatory, immunomodulatory and tissue regeneration functions (Tan et al. 2024). Therefore, we chose to use MSCs as the source cells for studying the molecular mechanisms regulating sEV secretion, where 3D culture conditions were created by loading MSCs onto microcarriers and growing these constructs in a 3D spinner flask bioreactor (Figure 1). We discovered that although knockdown of Rab27A and Rab27B could greatly reduce sEV secretion, their expression levels showed no significant differences between MSCs grown in 2D and 3D culture, suggesting that Rab27A and Rab27B were not the core regulators of sEV secretion. Remarkably, we found that cortical actin depolymerisation by cytoD or inhibition of ITGA1 greatly promoted sEV release by MSCs, elucidating a new regulatory mechanism for sEV production. Furthermore, we confirmed that sEVs derived from 3D MSC culture had superior therapeutic potential in osteoarthritis (OA) and wound healing in vivo models.

## 2 | Results

### 2.1 | 3D Culture of MSCs Increases sEV Secretion

MSCs cultured in the 3D bioreactor system (MSC-3D) underwent a stable proliferation phase in the first 2–3 days after cell seeding on microcarriers (microcryogels), following which the culture supernatant was collected between 4 and 9 days of culture at 3-day intervals (Figures 2a and S1). Scanning electron microscopy (SEM) images showed that MSC-3D adhered to the surface of microcarriers, with rapid proliferation seen over the first 5 days to completely cover the entire microcarrier surface (Figure 2b). CCK-8 assay indicated similar proliferation rates between MSCs grown in 2D (MSC-2D) and 3D (MSC-3D) over the first 3 days, with both groups showing an approximate 5-fold increase in cell number (Figure S2). With prolonged culture time, MSC-2D stopped proliferating after 3 days while MSC-3D continued to proliferate by up to 15-fold at 7 days, followed by a plateau in cell

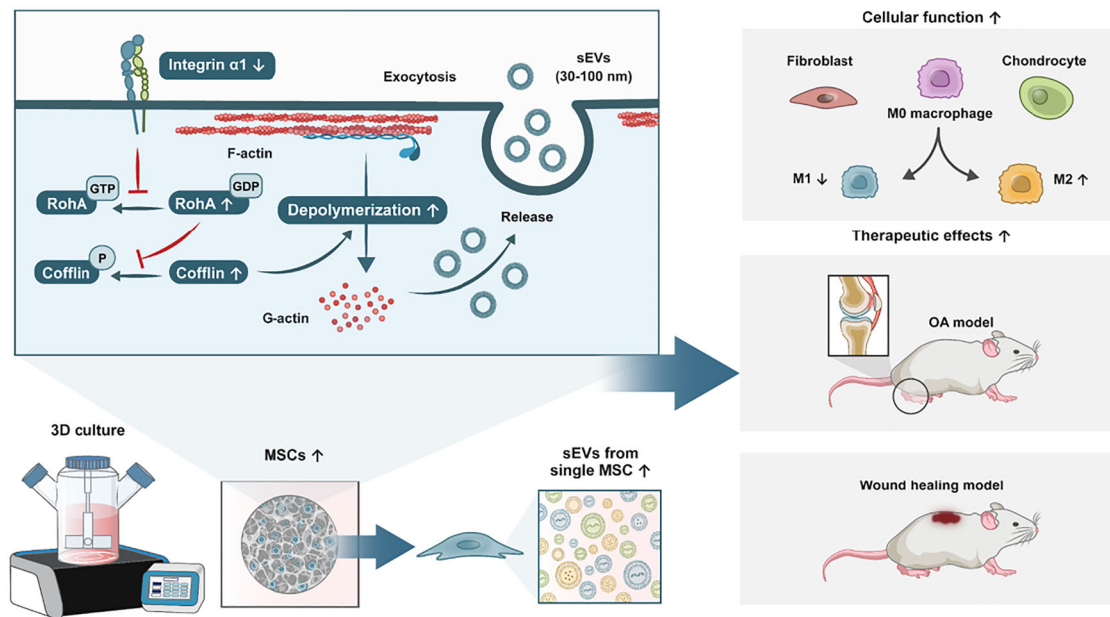


**FIGURE 1** | Schematic diagram of study design. MSCs, mesenchymal stem cells; EVs, extracellular vesicles; MVBs, multivesicular bodies; M1, represents type I macrophage; M2, represents type II macrophage; MSC<sup>2D</sup>-EVs, represent EVs derived from MSCs grown on a 2D plate; MSC<sup>3D</sup>-EVs, represent EVs derived from MSCs grown in a 3D culture system.

number from 7 to 15 days. Flow cytometry results showed that MSC-3D maintained higher expression levels of MSC-positive markers CD73, CD90 and CD105 compared to MSC-2D (Figure S3). Furthermore, MSC-3D showed significantly lower proportions of both senescent cells and apoptotic cells compared to MSC-2D (Figures S4 and S5).

sEVs were extracted from the culture supernatants of MSC-2D (MSC<sup>2D</sup>-sEVs) and MSC-3D (MSC<sup>3D</sup>-sEVs). Both MSC<sup>2D</sup>-sEVs and MSC<sup>3D</sup>-sEVs showed high expression of the sEV markers ALIX, CD63, TSG101 and CD9, as well as minimal expression of calnexin and GAPDH as markers of cellular contaminants (Figure 2c). Nanoparticle tracking analysis (NTA) indicated that the yield of MSC<sup>3D</sup>-sEVs was approximately 2.5 times higher than that of MSC<sup>2D</sup>-sEVs (Figure 2d). Transmission electron microscopy (TEM) showed a similar morphology between the MSC<sup>2D</sup>-sEVs and MSC<sup>3D</sup>-sEVs, where both groups appeared as spherical or elliptical small vesicles, but some might have exhibited a disk-like shape with a concave centre due to dehydration (Figure 2e).

MSC-2D and MSC-3D were then subjected to mRNA-seq analysis to compare global gene expression, from which 5494 differentially expressed genes (DEGs) were identified, including 2134 upregulated genes and 3360 downregulated genes (Figure S6a). Gene Ontology (GO) analysis indicated significant enrichment of pathways related to integrin-mediated signalling, integrin-mediated cell adhesion and the integrin complex (Figure 2f). There was notable enrichment in processes associated with GTPase activity, including GTP binding, GTPase activator activity, regulation of small GTPase-mediated signal transduction and GTP metabolic processes. Integrin-mediated processes, such as integrin binding, were also prominently represented. Furthermore, there was evidence of involvement by cytoskeleton metabolism-related processes, such as vesicle transport along

actin filaments and negative regulation of tubulin deacetylation. The analysis also revealed processes relating to the regulation of sEVs, including extracellular exosomes, extracellular vesicles, and the clathrin-coated endocytic vesicle membrane. Other regulatory mechanisms identified as being significant included those governing inflammatory responses, macrophage activation, chondrocyte differentiation and cartilage development.

KEGG analysis showed significant enrichment of MSC-3D in cytokine-cytokine receptor interaction, focal adhesion and ECM-receptor interaction (Figure 2g). Chord figures were used to explore the common DEGs enriched in integrin-related pathways and GTPase-related pathways (Figure S6b). In addition, the single-gene GSEA enrichment analysis of RhoA and its downstream target LIMK2 revealed significant enrichment of MSC-3D in biological processes and cellular components such as vesicle, stem cell, tubulin, and non-coding RNA (ncRNA) related pathways (Figure 2h,i). Other highly expressed genes in MSC-3D compared to MSC-2D included glycolytic-related genes (such as *HK2*, *PKM2* and *SAMP-2*), ESCRT-independent and GTPases genes (*Rab27a* and *Rab27b*), and ESCRT-dependent genes (*Stam-1*, *HRS*, *Alix* and *TSG10s1*) (Figure S7).

## 2.2 | Cortical Actin Depolymerisation Increases sEV Secretion Independent of Rab27A/B

Rab GTPases and cytoskeletal components, such as microtubules and actin filaments, have critical roles in regulating the secretion of sEVs (Colombo et al. 2014). To investigate whether sEV secretion from MSCs is regulated by Rab27A and Rab27B, these genes were knocked down in MSCs using small interfering RNA (siRNA). The optimal concentration for siRNA transfection in cells was determined (50 nM), and the knockdown (KD) efficiency was confirmed at multiple levels, including gene and



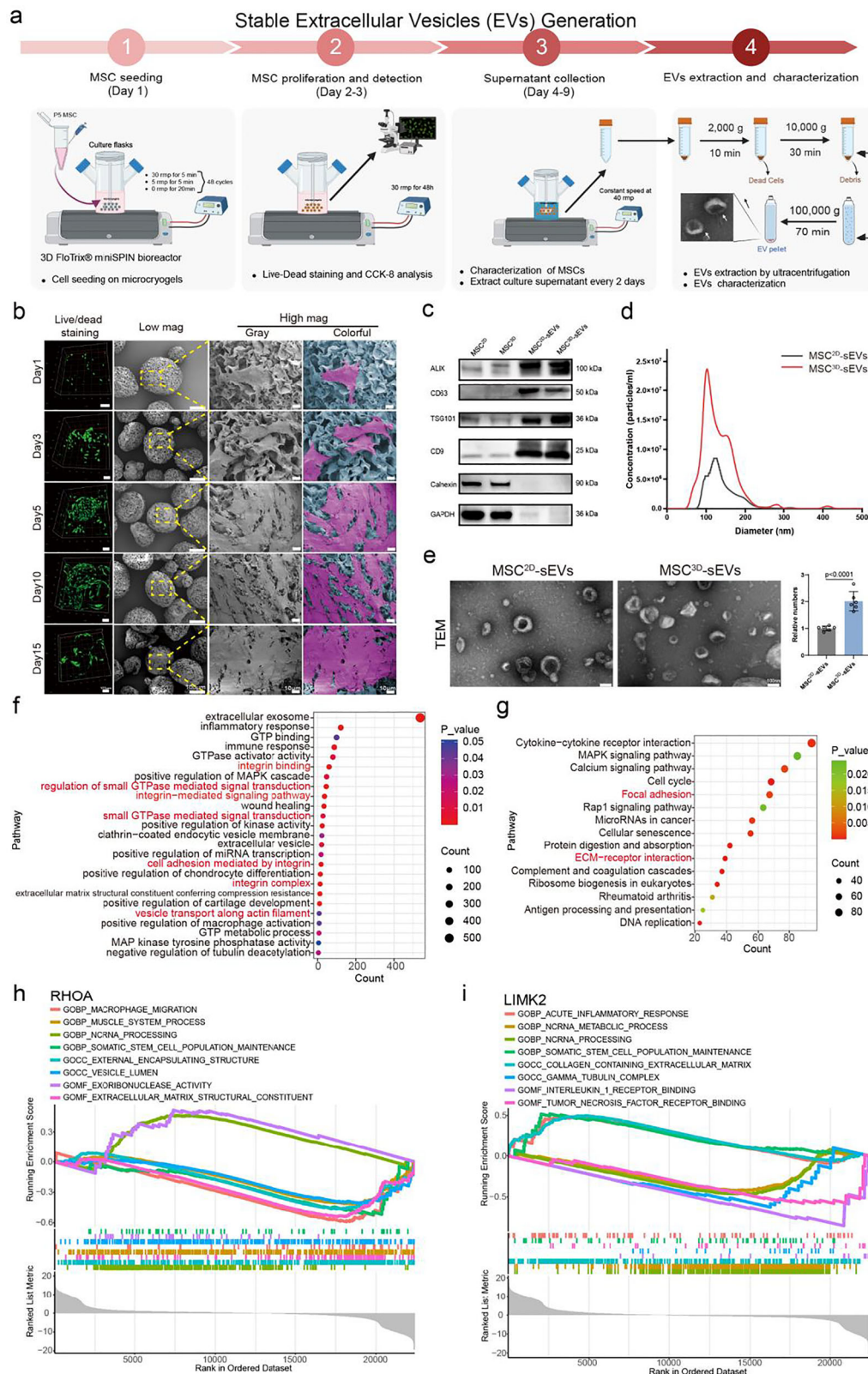


**FIGURE 2** | 3D culture of MSCs increases sEV secretion. (a) Schematic flow chart of 3D dynamic culture of MSCs and extraction of sEVs. (b) Live/dead staining and scanning electron microscopy (SEM) images of MSCs grown in 3D on microcryogels. (c) Western blotting (WB) results for sEV-specific markers CD9, Alix, TSG101 and CD63, along with the negative marker Calnexin. (d) Nanoparticle tracking analysis (NTA) showing the particle size distribution of sEVs derived from MSCs cultured in 2D (MSC<sup>2D</sup>-sEVs) and 3D (MSC<sup>3D</sup>-sEVs). (e) Representative transmission electron microscopy (TEM) images and semi-quantitative analysis of MSC<sup>2D</sup>-sEVs and MSC<sup>3D</sup>-sEVs. (f) Gene Ontology (GO) analysis of MSCs cultured on 2D plates and in 3D culture system. (g) KEGG analysis of MSCs cultured on 2D plates and in 3D culture system. (h) Gene Set Enrichment Analysis (GSEA) of RHOA in GO terms of macrophage migration, muscle system process, ncRNA processing, somatic stem cell population maintenance, external encapsulating structure, vesicle lumen, exoribonuclease activity and extracellular matrix structure constituent. (i) GSEA of LIMK2 in GO terms of acute inflammatory

protein (Figures 3a–c and S8–S10). NTA results indicated a significant reduction in sEV secretion by MSCs with Rab27A and Rab27B knockdown, confirming the pivotal role of Rab27 proteins in enabling the process of vesicle secretion (Figure 3d). We further examined the expression levels of Rab27A and Rab27B in MSC-2D and MSC-3D using immunostaining and western blot analysis (Figure 3e–g). Interestingly, 2D-SIM images revealed highly coincident spatial distribution of Rab27A and Rab27B with F-Actin (Figure 3a,e). This co-localisation suggests a possible role of Rab27A and Rab27B in facilitating efficient transport and release during sEV secretion by synergistically interacting with the cell cytoskeleton (Menaceur et al. 2023). Interestingly, our findings indicated similar levels of Rab27A and Rab27B expression in MSCs grown in 3D and 2D (Figure 3f,g), suggesting that increased sEV secretion by MSCs cultured in 3D is not primarily governed by changes in Rab27A and Rab27B expression. These observations prompted us to investigate other regulatory pathways responsible for enhanced sEV secretion in 3D-cultured MSCs.

The mRNA sequencing data led us to suspect cytoskeletal changes associated with F-actin as a possible regulatory mechanism for sEV secretion in 3D-cultured MSCs. We hypothesised that cortical actin depolymerisation might increase the secretion of sEVs, which we investigated by treating MSCs with an actin polymerisation inhibitor, cytochalasin D (cytoD). First, the optimal concentration and duration of cytoD stimulation on MSCs for inducing actin depolymerisation was determined to be 0.1  $\mu$ M cytoD for 4 h (Figure S11). We then compared the F-actin morphology in the 3D-MSC group to 2D-MSC, as well as to cells grown with DMSO and CytoD (Figure 3h). The 3D group showed irregular and disorganised F-actin morphology, accompanied by elevated G-actin content, which had similar appearance to the CytoD group but was distinctly different from the well-organised F-actin structures observed in the 2D and DMSO groups. These observations imply that a moderate reduction in cortical actin tension could potentially promote sEV secretion (Lenzini et al. 2021). Furthermore, we investigated the distribution of MVBs relative to the cytoskeleton by labelling them using a CD9 fluorescent probe. As a specific marker of sEVs, CD9 intensity in the 3D group was similar to the CytoD group and showed distribution primarily around the cell nucleus, but was markedly lower in the 2D and DMSO groups (Figure 3i). Meanwhile, time-lapse images of live cells revealed further similarities between the 3D and CytoD groups, with both showing more active motility of MVBs compared to the 2D and DMSO groups (Figure 3j, Movie S1–S4). TEM images of sEVs derived from different groups of MSCs revealed similar vesicle morphology between groups (Figure 3k). Concurrently, the NTA results demonstrated elevated sEV secretion in 3D-MSC and CytoD groups (Figure 3l), particularly after sEV secretion was normalised to cell number (Figure 3m). These results collectively indicate that increased sEV secretion in 3D as opposed to 2D cultured MSCs is driven by cortical actin depolymerisation, a process mimicked by the addition of cytoD. This enhanced sEV secretion is independent of Rab27A/B regulation, and results in elevated yield of sEVs from 3D-MSC without affecting vesicle size or morphology.

### 2.3 | ITGA1/RhoA/Cofilin Pathway Downregulation Promotes Cortical Actin Depolymerisation and sEV Secretion

Having identified cortical actin depolymerisation as a key mechanism that increases sEV secretion in 3D cultured MSCs, we then sought to elucidate the upstream molecular pathways regulating these cytoskeletal changes. Based on the analysis of DEGs between MSC-2D and MSC-3D, we centred on the differential expression of integrin family members. We chose to focus on integrins that were significantly downregulated in MSC-3D, given their role in cytoskeletal aggregation upon ligand-receptor binding (Figure 4a). Considering the *p* value and basal gene expression levels, we selected integrin  $\alpha 1$  (ITGA1) as the upstream target for further investigation, which demonstrated significant enrichment in GTPase-related pathways (Figure 4b–c). We first determined the optimal concentration of ITGA1 antibody for inducing MSC cytoskeletal remodelling, and found that 10  $\mu$ g/mL was sufficient to significantly alter the entire cell adhesion process as well as post-adhesion morphology (Figure S12). Blocking ITGA1 in MSCs was found to result in significant depolymerisation of F-actin into G-actin, accompanied by increased distribution of MVBs along the cytoskeleton and abutting the plasma membrane, suggesting a greater potential for sEV release (Figure 4d–e). Meanwhile, MSC-3D showed significantly lower distribution of ITGA1 on the cell membrane compared to the MSC-2D, DMSO and CytoD groups (Figure 4f). It would appear from these findings that ITGA1 expression in MSCs is diminished in 3D culture conditions, subsequently leading to cortical actin depolymerisation that results in enhanced sEV secretion.

Based on the results of single-gene GSEA enrichment analysis of RhoA and its downstream target LIMK2, we investigated the RhoA/cofilin signalling pathway as a potential regulator mediating the effects of altered ITGA1 expression in MSCs on cortical actin (de)polymerisation. Western blot analysis showed significantly lower protein expression of ITGA1 in the 3D-MSC and ITGA1 blocked groups compared to the 2D-MSC, DMSO and CytoD groups (Figures 4g–h). While total RhoA expression was similar among the five groups, the activated form of RhoA (RhoA-GTP) showed significantly lower expression in the 3D-MSC and ITGA1 blocked groups compared to the 2D-MSC, DMSO and CytoD groups. A similar trend was observed for cofilin, where total cofilin expression was similar among all groups but the phosphorylated form of cofilin (p-cofilin) was significantly lower only in the 3D-MSC and ITGA1 blocked groups. For actin expression, a similar level of total actin (T-actin) was found between groups, but the level of F-actin in the 3D-MSC, CytoD and ITGA1 blocked groups was significantly lower than the 2D and DMSO groups. This was accompanied by exactly the opposite expression pattern for G-actin. TEM images taken to illustrate sEV secretion from MSCs in different groups showed an increased number of fusion events between MVBs and the plasma membrane in MSC-3D, which was in alignment with enhanced sEV secretion from this group (Figures 4i). A similar



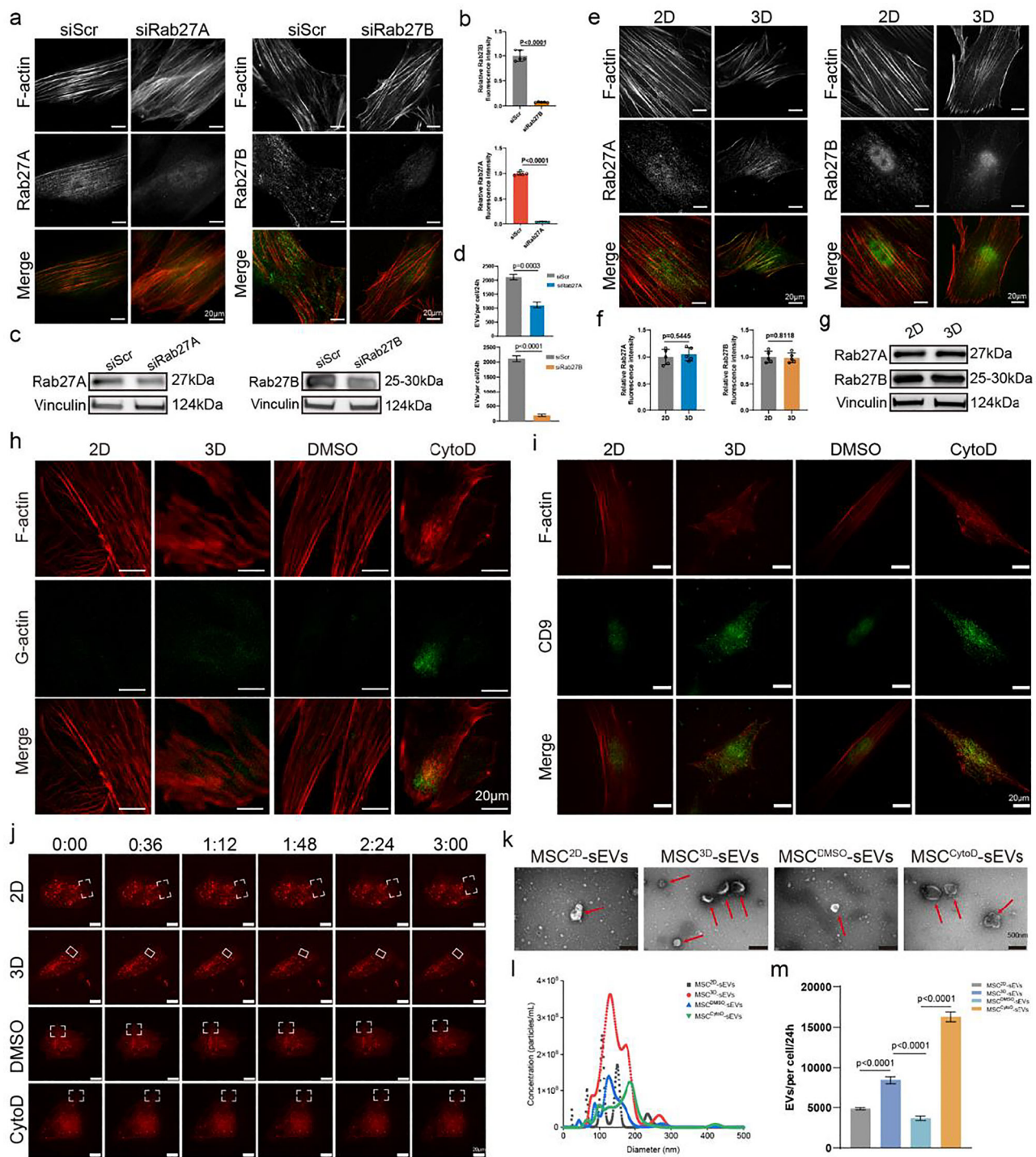


**FIGURE 3** | Cortical actin depolymerisation increases sEV secretion independent of Rab27A/B. (a) Representative 2D-SIM immunofluorescence staining images of Rab27A, Rab27B and F-actin after siRNA knockdown of Rab27A and Rab27B. (b) Semi-quantitative analysis of Rab27A and Rab27B in immunofluorescence staining images following transfection ( $n = 5$ ). (c) Representative results of western blot analysis for the expression of Rab27A and Rab27B in MSCs after siRNA knockdown. Vinculin was used as a loading control. (d) Number of secreted sEVs normalised to the cell number. (e) Representative 2D-SIM immunofluorescence staining images of Rab27A, Rab27B and F-actin in 3D and 2D cultures. (f) Semi-quantitative analysis of Rab27A and Rab27B immunofluorescence staining images in 3D and 2D cultures ( $n = 5$ ). (g) Representative results of western blot analysis for the expression of Rab27A and Rab27B in 3D and 2D cultures. Vinculin was used as a loading control. (h) Representative immunofluorescence staining images of G-actin and F-actin of MSCs cultured in different conditions. (i) Representative immunofluorescence staining images of CD9 (specific marker of sEVs) and F-actin of MSCs cultured in different conditions. (j) Cell membrane of MSCs cultured under different conditions were pre-labelled with a live cell dye, and time-lapse sequence photographs of live cells were taken at 5-s intervals to obtain time-lapse sequence maps. (k) Representative TEM images of different sEVs. (l) Nanoparticle tracking analysis (NTA) showing the particle size distribution of different sEVs. (m) Number of secreted sEVs in different groups normalised to the cell number.

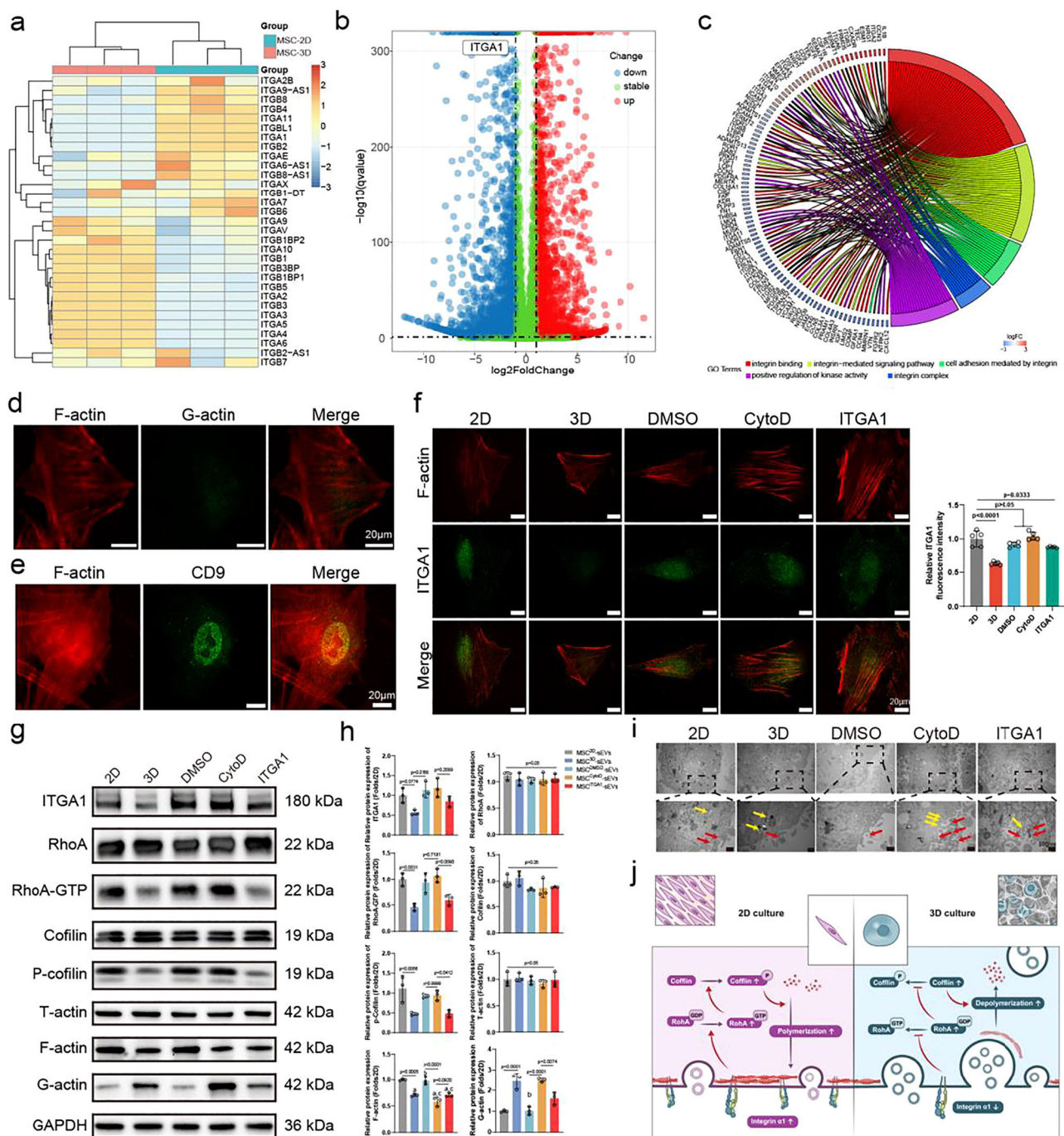


**FIGURE 4** | ITGA1/RhoA/cofilin pathway downregulation promotes cortical actin depolymerisation and sEV secretion. (a) Heatmap representation of Differentially Expressed Genes (DEGs) in MSC-2D and MSC-3D. (b) Volcano diagram highlighting DEGs. (c) Circular plot of DEGs mainly associated with integrin binding, integrin-mediated signalling pathway, cell adhesion mediated by integrin, positive regulation of kinase activity and integrin complex. (d) Representative immunofluorescence staining images of G-actin and F-actin in MSCs with blocked ITGA1. (e) Representative immunofluorescence staining images of CD9 and F-actin in MSCs with blocked ITGA1. (f) Representative immunofluorescence staining images of ITGA1 and F-actin in MSCs cultured in different conditions. (g) Representative western blots and (h) Corresponding quantification for the expression of RhoA, RhoA-GTP, cofilin, p-cofilin, T-actin, F-actin and G-actin in MSCs cultured in different conditions. The insoluble F-actin pool was separated from the soluble G-actin pool using Triton-X100 extraction and subsequent centrifugation. GAPDH was used as a loading control. (i) Representative TEM images of sEV secretion from MSCs in different conditions. (j) Schematic illustrating the potential mechanism regulating sEV secretion from MSCs cultured in a 3D environment. Inhibition of the integrin  $\alpha 1$  (ITGA1) receptor reduces activation of the RhoA/cofilin pathway, thereby preventing actin polymerisation from G-actin to F-actin, and promoting the transportation and secretion of multivesicular bodies (MVBs) from the cell into the extracellular space. CytoD, cytochalasin D; integrin  $\alpha 1$ : ITGA1; MVBs: multivesicular bodies.



pattern was seen in the CytoD and ITGA1 blocked groups, while in contrast, the MSC-2D and DMSO groups showed limited sEV secretion. Concurrently, trends in the levels of sEV secretion across groups were verified by NTA (Figure S13). Connecting the dots, we propose that 3D culture results in downregulation of ITGA1 in MSCs, which in turn attenuates the activation of the RhoA/cofilin signalling pathway (Figure 4j). This then leads to moderate depolymerisation of the cortical actin cytoskeleton, facilitating increased MVB fusion with the plasma membrane and hence the secretion of sEVs into the extracellular space.

## 2.4 | MSC<sup>3D</sup>-sEVs Enhance Cell Activity and Macrophage Polarisation Compared to MSC<sup>2D</sup>-sEVs

Having elucidated the pathways by which 3D culture increases sEV yield in MSCs, we then sought to compare the differences in therapeutic function between sEVs produced by MSC-3D and MSC-2D. We chose chondrocytes and human dermal fibroblasts (HDFs) as in vitro cell models, in line with later in vivo testing, to assess cell proliferation, migration and anti-senescence activity after treatment with MSC<sup>3D</sup>-sEVs and MSC<sup>2D</sup>-sEVs (Figure 5a). EdU assay was used to measure the proportion of proliferative chondrocytes and HDFs, which was found to be approximately 16% and 9%, respectively, for cells treated with MSC<sup>2D</sup>-sEVs, which increased to approximately 30% and 15%, respectively, for cells treated with MSC<sup>3D</sup>-sEVs (Figure 5b,c). CCK-8 assay also demonstrated a significant increase in the proliferation of chondrocytes and HDFs treated by MSC<sup>3D</sup>-sEVs compared to MSC<sup>2D</sup>-sEVs from days 4 to 7 onwards (Figure S14). Interestingly, although chondrocyte and HDF proliferation were similar between the 2D and 3D sEV groups at day 1, both cell types showed greatly elevated migration after 24 h treatment with MSC<sup>3D</sup>-sEVs, evidenced by a significant reduction in gap area from the scratch wound healing assay compared to cells treated with MSC<sup>2D</sup>-sEVs (Figure 5d,e). For chondrocytes, the gap area for the MSC<sup>3D</sup>-sEVs and MSC<sup>2D</sup>-sEVs groups was 36% and 52%, respectively, which reduced to 4% and 30% after 48 h. For HDFs, these numbers were 29% and 45%, respectively, for MSC<sup>3D</sup>-sEVs and MSC<sup>2D</sup>-sEVs at 24 h, and 18% and 28% at 48 h. The ability of MSC<sup>3D</sup>-sEVs to enhance the migration of chondrocytes and HDFs after stimulation for 24 h was separately confirmed through transwell assays (Figure S15). In addition, MSC<sup>3D</sup>-sEVs were more effective in reducing the proportion of senescent cells compared to MSC<sup>2D</sup>-sEVs. SA- $\beta$ -Gal staining, a marker of cell senescence, was markedly higher in the control group compared to sEV-treated groups for both chondrocytes and HDFs (Figure 5f–g). The percentage of SA- $\beta$ -Gal positive cells was 33%, 12% and 5%, respectively, for the control, MSC<sup>2D</sup>-sEVs, and MSC<sup>3D</sup>-sEVs groups in chondrocytes, and 24%, 15% and 9%, respectively, in HDFs.

Since inflammation is a common aetiology underlying chronic diseases, we compared the immunomodulatory capabilities of sEVs from 2D and 3D cultured MSCs on rat bone marrow-derived macrophages (BMDMs). The results from qPCR analysis indicated significant downregulation of gene expression associated with M1 macrophage polarisation (CD86, TNF- $\alpha$ , iNOS and IL-1 $\beta$ ) in BMDMs treated with MSC<sup>3D</sup>-sEVs compared to MSC<sup>2D</sup>-sEVs, accompanied by significant upregulation of genes associated with M2 macrophage polarisation (CD206, IL-4, IL-10

and Arg-1) (Figure 5h). As additional indicators of M1 (CD86) and M2 (mannose) macrophage polarisation, BMDMs treated with MSC<sup>3D</sup>-sEVs and MSC<sup>2D</sup>-sEVs, respectively, showed 3.80% and 17.39% of cells expressing CD86, and 58.77% and 32.61% of cells expressing mannose (Figure 5i).

MicroRNA (miRNA) sequencing was conducted to gain a better understanding of the molecular basis by which sEVs from 3D cultured MSCs improve cellular anabolism and modulate macrophage polarisation (Figure S16). We identified the top 5 miRNAs exhibiting the most significant differences in expression between the 3D and 2D groups: miR-181b-5p, miR-4802-3p, miR-664a-5p, miR-27a-5p and miR-4491 (Figure S16a,b). We found that 474 DEGs were highly expressed in MSC<sup>3D</sup>-sEVs (Figure S16c). GO enrichment analysis of these target genes showed that MSC<sup>3D</sup>-sEVs were primarily involved in the regulation of wound healing, macrophage differentiation, and cartilage development, which was consistent with the enrichment results in our bulk RNA-seq of MSCs (Figure S16d). KEGG enrichment analysis showed that the most likely pathways by which MSC<sup>3D</sup>-sEVs exerted their effects on cells were related to the regulation of cellular senescence, regulation of pluripotency of stem cells, MAPK, mTOR, TGF- $\beta$ , and PI3K-Akt signalling pathways (Figure S16e). Finally, a comparison of qPCR analysis of the top 5 miRNA candidates revealed that miR-181b-5p, miR-664a-5p and miR-4491 exhibited significant differences between the 2D and 3D sEV groups, suggesting their potential roles as the core miRNA species involved in the regulatory functions of MSC<sup>3D</sup>-sEVs (Figure S17).

## 2.5 | In Vivo Effects of MSC<sup>3D</sup>-sEVs Treatment in OA Rats

Having confirmed that 3D culture of MSCs can increase both yield and in vitro therapeutic function of sEVs, it was important to investigate whether the same beneficial effects can be carried to in vivo chronic disease models. In line with the cell models we used for in vitro testing, we chose to investigate the in vivo treatment effects of sEVs derived from 2D and 3D cultured MSCs in rat models of osteoarthritis (OA) and wound healing, both of which are highly prevalent diseases that would benefit from improved treatment options.

The rat OA model was created by ACL transection (Figure S18), followed by two injections of treatment groups given at 2 and 4 weeks post-surgery (Figure 6a), with subsequent analyses performed at 6 weeks after the initial surgery. At the time of analysis, the group treated with MSC<sup>2D</sup>-sEVs showed an increase in paw contact area, as well as improvements in ground pressure and contact time compared to the PBS group, suggesting partial relief of knee joint pain (Figure 6b,c). Meanwhile, rats treated with MSC<sup>3D</sup>-sEVs exhibited the largest footprint area, with ground pressure and contact time greatly exceeding those treated with MSC<sup>2D</sup>-sEVs and approaching the gait characteristics of normal rats (Figures 6c and S19). X-ray and  $\mu$ -CT imaging indicated narrowing of the intercondylar notch and increased osteophyte formation in the medial femoral condyle and tibial plateau of the PBS group, suggestive of OA progression (Figure 6d). These pathological changes were partly attenuated in the MSC<sup>2D</sup>-sEVs group and significantly attenuated in the MSC<sup>3D</sup>-sEVs group, where the latter showed significantly increased joint space



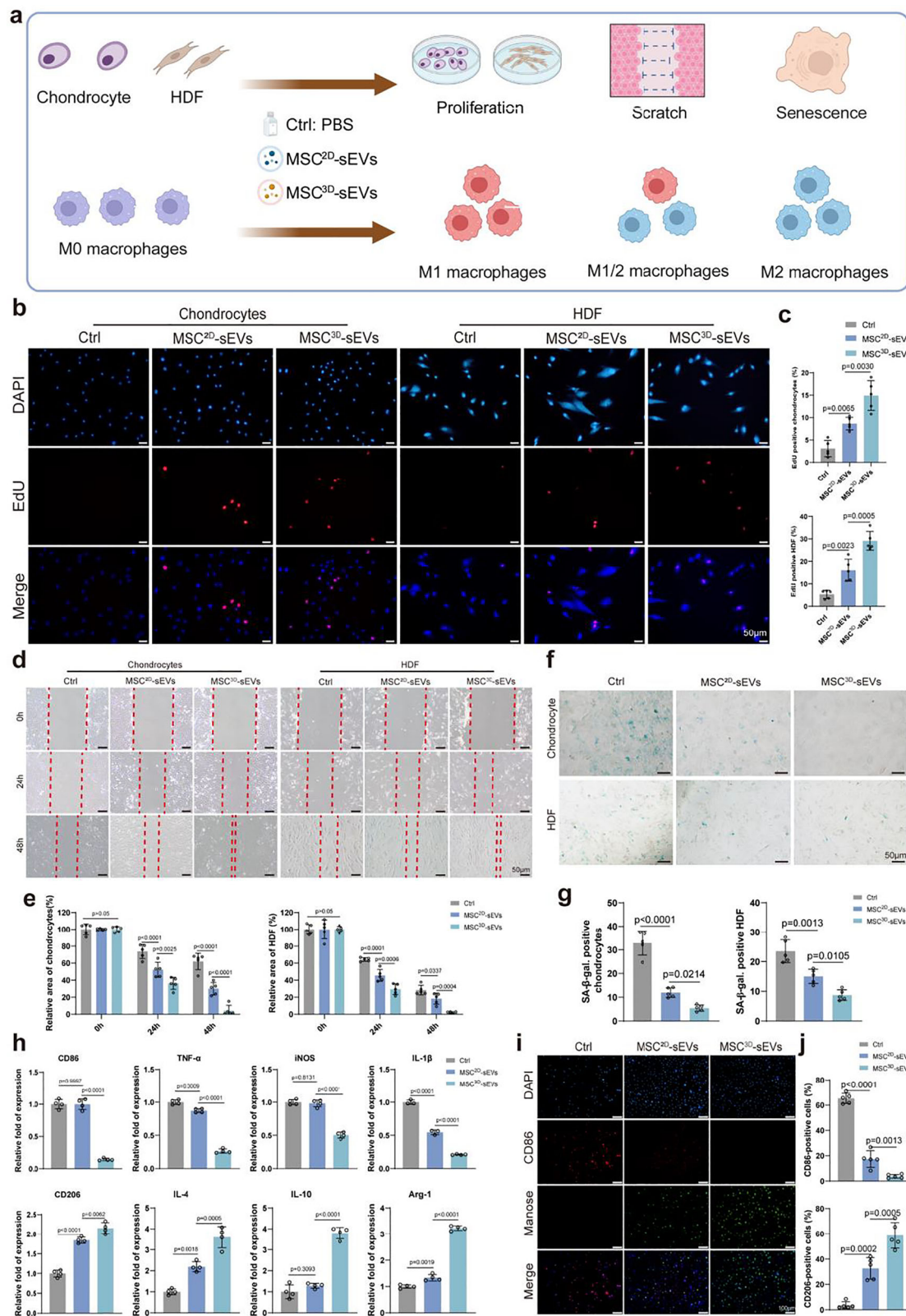


**FIGURE 5** | MSC<sup>3D</sup>-sEVs enhance cell activity and macrophage polarisation compared to MSC<sup>2D</sup>-sEVs. (a) Schematic illustrating the experiments using different groups of sEVs to evaluate their effects on the proliferation, migration and anti-senescence activity of chondrocytes and human dermal fibroblasts (HDFs). (b) EdU staining and (c) semi-quantitative analysis of cells treated with different sEV groups. (d) Scratch wound healing assay, and (e) Semi-quantitative analysis of scratch gaps in different groups ( $n = 5$ ). (f) Representative images of SA-β-Gal staining in chondrocytes and HDFs, and (g) Percentage of SA-β-Gal<sup>+</sup> cells ( $n = 5$ ). (h) Relative gene expression of M1-related genes (CD86, TNF-α, iNOS and IL-1β) and M2-related genes (CD206, IL-4, IL-10 and Arg-1). (i) Immunofluorescence staining and (j) Semi-quantitative analysis of CD86 and mannose expression.

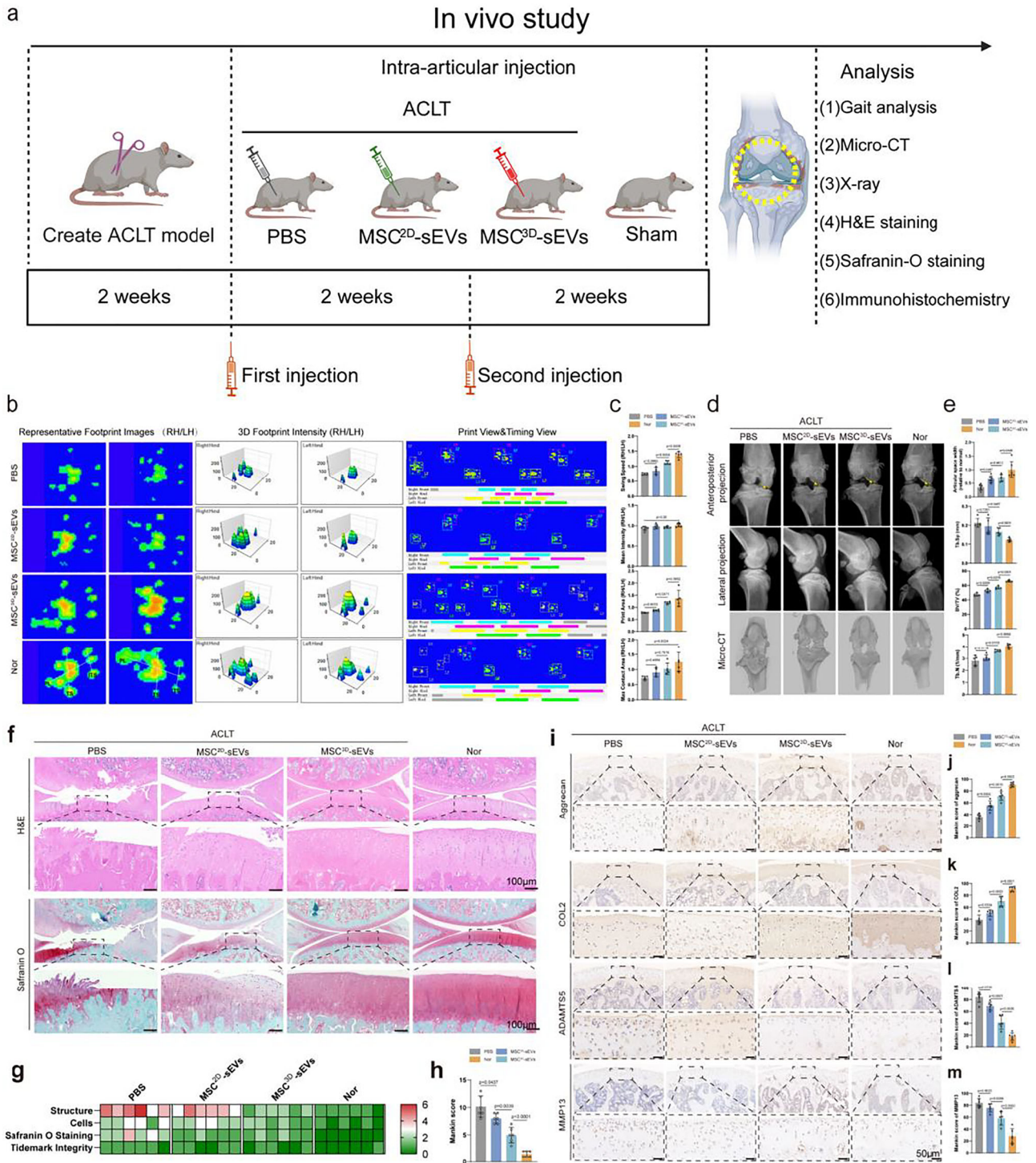


**FIGURE 6** | In vivo effects of MSC<sup>3D</sup>-sEVs treatment in OA rats. (a) Schematic illustration of establishing the rat OA model, and experimental design for evaluating the protective effects of different sEVs. (b) Representative footprint images and 3D footprint intensity (RH/LH) ( $n = 5$ ). (c) Evaluation of swing speed, mean intensity, print area, and maximum contact area during walking. (d) X-ray and 3D reconstructed  $\mu$ -CT images. (e) Quantitative analysis of articular space width, trabecular separation (Tb.Sp), bone volume fraction (BV/TV), and trabecular number (Tb.N) from  $\mu$ -CT ( $n = 5$ ). (f) H&E and safranin-O staining of joint sections at 6 weeks post-surgery. (g) Heatmap representation of Mankin scoring for joint histopathology. (h) Quantitative Mankin score analysis of safranin-O staining. (i) Immunohistochemical staining of aggrecan, collagen II (COL2), ADAMTS5 and MMP13. (j) Quantitative Mankin score analysis of aggrecan staining. (k) Quantitative Mankin score analysis of COL2 staining. (l) Quantitative Mankin score analysis of ADAMTS5 staining. (m) Quantitative Mankin score analysis of MMP13 staining ( $n = 6$ ).



widening, decreased number of osteophytes, and higher values of BV/TV and Tb.N (Figure 6e).

Histological staining with H&E and safranin-O confirmed OA progression in the PBS group, as shown by severe cartilage destruction and loss of glycosaminoglycans (GAGs) (Figure 6f). Compared to the MSC<sup>2D</sup>-sEVs group, the MSC<sup>3D</sup>-sEVs group showed a smoother cartilage surface approaching normal (sham) cartilage morphology and GAG content. Quantitative analysis using Mankin scores showed similar trends, where the highest score seen in the PBS group confirmed a high degree of cartilage degeneration, followed by improvement in the MSC<sup>2D</sup>-sEVs group and significant score reduction in the MSC<sup>3D</sup>-sEVs group (Figure 6g,h). The results of immunohistochemical staining and associated Mankin scores displayed similar trends, where the MSC<sup>3D</sup>-sEVs group achieved the highest expression of the cartilage anabolic markers aggrecan and COL2 among the treatment groups, accompanied by lowest expression of the catabolic markers ADAMTS5 and MMP13 (Figure 6i-m). These findings suggest that sEVs derived from MSCs cultured in 3D have a superior capacity to maintain cartilage homeostasis and delay OA progression after injury compared to MSC-sEVs from 2D culture.

## 2.6 | In Vivo Effects of MSC3D-sEVs Treatment on Wound Healing in Rats

The rat wound healing model was created by inflicting a large skin wound (Figure S20), followed immediately by implantation of a GelMA hydrogel (for immobilising the treatment) loaded with PBS, MSC<sup>2D</sup>-sEVs or MSC<sup>3D</sup>-sEVs (Figure 6a), with analyses performed over a period of 14 days. The macroscopic views of tissue healing showed relatively large wound areas throughout the 14-day period in the untreated control and PBS groups, indicating incomplete healing (Figure 7b). Meanwhile, the MSC<sup>3D</sup>-sEVs group showed the most accelerated wound healing rate among all groups, and greatly exceeded the MSC<sup>2D</sup>-sEVs group. The same trends were demonstrated by semi-quantitative analysis of final healing area, which reached 94.58% in the MSC<sup>3D</sup>-sEVs group compared to 89.12% for MSC<sup>2D</sup>-sEVs, 75.85% for PBS and 72.06% for the untreated control (Figure 7c). Histologically, the control and PBS groups exhibited notable depressions at the injury site, accompanied by newly formed tissue that showed incomplete defect filling, predominantly comprised disorganised fibrous tissue, had poor integration with surrounding normal skin, and lacked a distinct stratum corneum layer (Figure 7d). In contrast, the MSC<sup>3D</sup>-sEVs group showed almost complete defect filling and formation of new tissue with cell morphology and collagen arrangement closely mimicking normal skin, whereas these effects were less pronounced in the MSC<sup>2D</sup>-sEVs group. Semi-quantitative analysis of hair follicle numbers and wound length also showed the highest and lowest values, respectively in the MSC<sup>3D</sup>-sEVs group compared to other treatment groups (Figure 7e). These findings suggest that sEVs from 3D cultured MSCs were effective in promoting in vivo skin wound healing, with better restoration of both tissue structure and function compared to sEVs from MSCs grown in 2D culture.

## 3 | Discussion

Despite their immense therapeutic potential and ability to circumvent the practical limitations of live cell injection, EVs have experienced hurdles in upscaling into clinically applicable therapies due to the often unrealistic numbers of source cells required to generate sufficient EV doses (Pincela Lins et al. 2023). 3D culture systems, including various bioreactors, have recently been used to generate EVs from MSCs, and were generally reported to be effective at increasing the EV yield (Yuan et al. 2022; Yan and Wu 2020; Cao et al. 2020; Jeske et al. 2023). However, heterogeneous study design and the lack of mechanistic investigations make it difficult to understand the drivers behind increased EV yield in 3D culture systems, and hence how to better harness these systems for standardised EV production in future clinical applications. In this study, we employed a 3D culture system comprising microcarrier-based MSC culture in spinner flask bioreactors, which was found to greatly increase both yield and therapeutic function of MSC-derived sEVs. We investigated the detailed mechanism by which 3D culture enhanced sEV secretion from MSCs, and discovered that cortical actin depolymerisation in the cell cytoskeleton played a major role, a process that was independent of Rab27A/B regulation. Upstream of this, we further showed that 3D culture could downregulate the surface expression of integrin- $\alpha 1$  (ITGA1) in MSCs, thereby inhibiting RhoA/cofilin signalling pathway activation and in turn increasing cortical actin depolymerisation. This novel mechanism regulating sEV secretion is illustrated in Figure 1. Moreover, we confirmed that sEVs derived from 3D cultured MSCs had enhanced therapeutic function in both in vitro and in vivo models relevant to two examples of chronic diseases—OA and wound healing.

3D dynamic bioreactors, such as miniaturised dynamic wave-motion and vertical-wheel bioreactors, have recently been used for 3D culture of MSCs as cell aggregates, spheroids, and microcarrier constructs (Borys et al. 2020; Wang et al. 2022). In this study, we chose a well-established 3D cell culture platform comprising gelatin microcarriers as a cell culture vehicle together with a spinner flask bioreactor system to facilitate 3D dynamic culture conditions through biomimetic stirring and micromechanical stimulation (Li et al. 2014). Our previous findings indicated that this 3D culture system could sustain MSCs in a metabolically favourable state, leading to improved proliferative activity, stemness, paracrine function and protection against senescence and apoptosis compared to cells grown in 2D (Wang et al. 2022; Xing et al. 2020). Consistent with our findings, other studies have also suggested that 3D culture can induce structural and functional changes in MSCs, including activation of autophagy, enhancement of anti-senescence properties and alterations in cellular morphology and cytoskeletal dynamics (Mo et al. 2018; Jeske et al. 2023). MSCs grown using the 3D culture system in this study demonstrated greatly elevated sEV secretion per cell, by approximately two-fold compared to cells grown on 2D plates, which was in good alignment with previous reports showing increased EV secretion in 3D cultured MSCs that was approximately 2–20 times higher than 2D cultured cells (Yuan



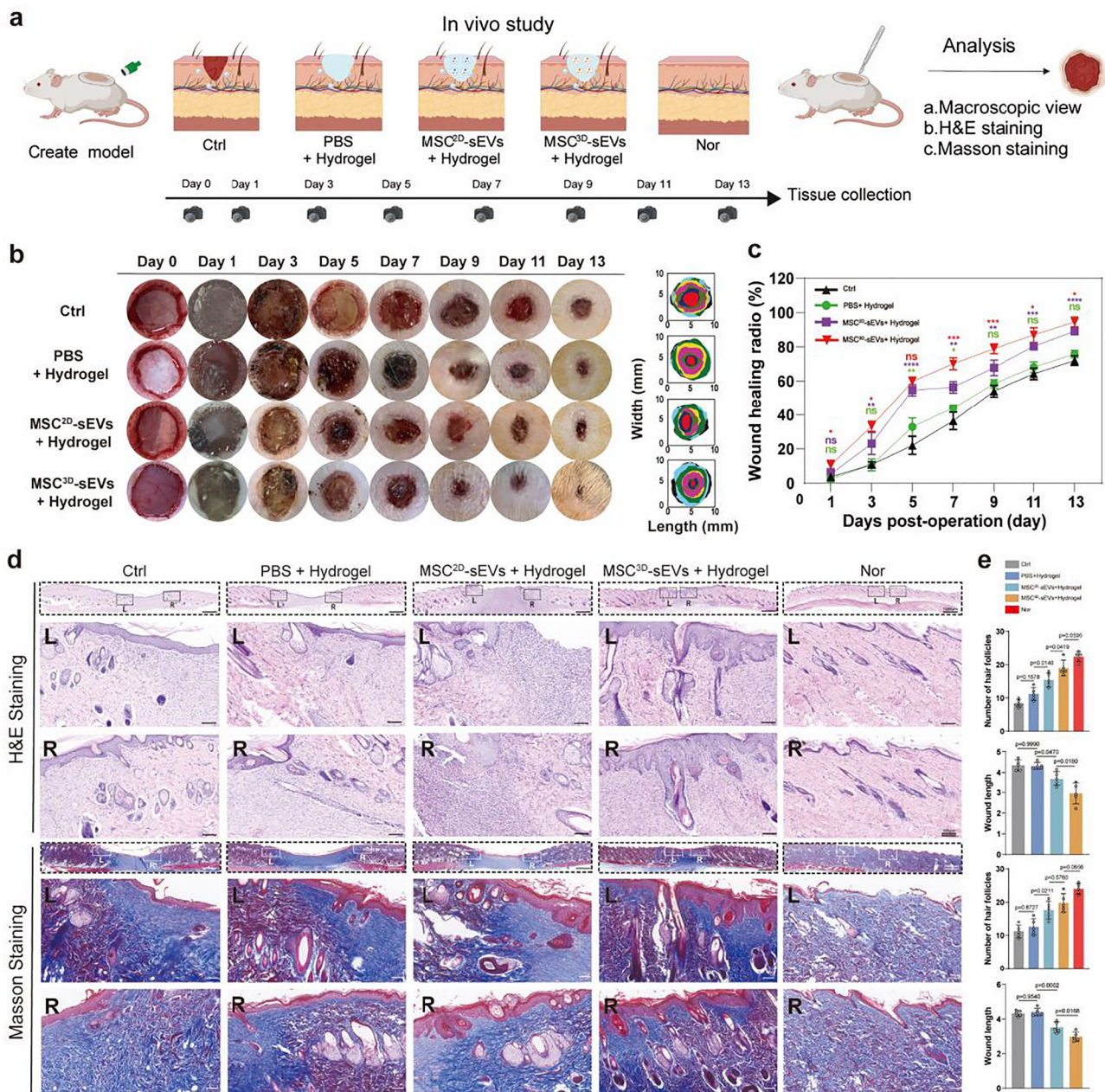


**FIGURE 7** | In vivo effects of MSC<sup>3D</sup>-sEVs treatment on wound healing in rats. (a) Schematic illustration of the rat wound healing model. (b) Representative images depicting the dynamic progress of wound healing in different groups on days 0, 1, 3, 5, 7, 9, 11 and 14. (c) Wound healing ratio on days 0, 1, 3, 5, 7, 9, 11 and 14 ( $n = 5$ ). (d) H&E and Masson staining with semi-quantitative analysis of the wound tissue on day 14.

et al. 2022; Yan and Wu 2020; Cao et al. 2020; Jeske et al. 2023). Various external cues including hypoxia, pH, drug stimulation and substrate stiffness, have been reported to affect the secretion, cargo and composition of sEVs (Liu and Su 2019; Jeyaram et al. 2020). Some evidence also suggests that in 3D culture systems comprising both static 3D stimulation provided to cells by microcarrier culture and dynamic 3D stimulation provided by a bioreactor, the dynamic environment and shear forces from the latter had more significant contribution to modulating sEV cargo and secretion from MSCs (Jeske et al. 2023). However, the molecular mechanisms driving increased sEV secretion from MSCs grown in a dynamic 3D culture system have not been clearly defined.

sEVs originate from inward budding of the plasma membrane, forming early endosomes that mature into MVBs. The ESCRT machinery is a key player in regulating the upstream processes prior to sEV release, by facilitating the sorting and packaging of cargo into ILVs. Other ESCRT-independent mechanisms, involving lipids such as ceramide, also play significant roles in sEV formation (Han et al. 2022). In addition, Rab GTPases such as Rab27A/B have crucial functions in directing the transport of MVBs along the cell cytoskeleton, determining their destination as either towards the plasma membrane for secretion or towards lysosomes for degradation (Han et al. 2022; Ostrowski et al. 2010). In particular, Rab27A/B regulates the movement of MVBs along the cytoskeleton towards the plasma membrane, facilitating

their docking and fusion with the membrane by interacting with effector proteins such as Slp4 and Munc13-4 (Pfeffer 2010). These interactions are essential for the subsequent release of sEVs in various secretory cells, including acinar epithelial cells, melanocytes, oligodendrocytes, and HeLa cells (Ostrowski et al. 2010; Chiang et al. 2011; Guo et al. 2019; Bello-Morales et al. 2012). However, it remains unclear whether Rab27A/B can regulate the release of sEVs in MSCs. Our findings indicated that knockdown of Rab27A or Rab27B significantly reduced the number of sEVs produced per cell in MSCs, confirming a central regulatory role of Rab27A/B in sEV secretion from MSCs akin to other cell types. Interestingly, we also found that MSCs grown in 3D had similar Rab27A/B protein expression levels as cells grown in 2D, despite the former having a significantly higher yield of sEVs. These observations suggested that the mechanisms leading to increased sEV secretion by 3D cultured MSCs were not related to MVB transport and docking processes regulated by Rab27A/B.

Cortical actin forms part of the cell cytoskeleton, comprising a dense network of actin filaments beneath the plasma membrane. It may act as a facilitator or barrier to sEV secretion from the cell depending on its state of polymerisation (Gowrishankar et al. 2012). Cortical actin can facilitate sEV release by providing structural support for vesicle transport and guiding secretory vesicles to docking sites at the plasma membrane (Ritter et al. 2017; Sinha et al. 2016). Conversely, excessive cortical actin polymerisation can impede sEV release by restricting vesicle access to the plasma membrane, thus preventing exocytosis (Papadopoulos et al. 2015; Trifará et al. 2008). The influence of cortical actin polymerisation on sEV secretion is governed by a fine balance, where vesicle secretion can be enhanced by the partial depolymerisation of actin filaments, but impeded by complete filament disassembly (Mo et al. 2018; Mitchell et al. 2008). Experimentally, the actin polymerisation inhibitor cytoD may be used to replicate these interactions, whereby low concentrations of cytoD (0.8–2  $\mu$ M) have been found to increase EV secretion and a high cytoD dose (10  $\mu$ g/mL) has been shown to reduce EV release (Mo et al. 2018; Headland et al. 2014). In this study, we found that cytoD treatment at 0.1  $\mu$ M for 4 h was optimal for inducing actin depolymerisation in MSCs and subsequently increasing the total amount of sEV release. Interestingly, we found that MSCs grown in 3D culture exhibited actin depolymerisation to a similar extent as cells exposed to cytoD, with comparable disorganisation in F-actin and elevation in G-actin. These observations pointed us to hypothesise that 3D culture might enhance sEV release from MSCs by increasing cortical actin depolymerisation, and to investigate the upstream regulatory mechanisms leading to these effects.

The Rho/cofilin axis is a key player in the regulation of cytoskeletal dynamics (Yu et al. 2020; Lin et al. 2003; Han et al. 2020; Quast et al. 2009). Rho is directly involved in integrin-mediated signalling by switching between an active GTP-bound state and an inactive GDP-bound state (Takai et al. 2001; Ridley 2001). It also regulates the actin cytoskeleton by activating Rho-associated kinases ROCK I and II (collectively referred to as ROCK), which in turn modulate various downstream effectors, with LIM kinase (LIMK) being a key mediator (Narumiya et al. 2009). Following

its activation by ROCK, LIMK phosphorylates cofilin on its serine 3 residue, effectively suppressing actin depolymerisation (Schmandke et al. 2007). The activity of cofilin is modulated by its phosphorylation state, which may either facilitate the severing and depolymerisation of actin filaments or inhibit cytoskeletal degradation and promote polymerisation (Bernstein and Bamberg 2010; Wang et al. 2007). Emerging evidence has suggested that the combined Rho/ROCK/LIMK/cofilin axis plays an important role in regulating the dynamic changes of the actin-based cytoskeleton (Hitsuda et al. 2022), although this has most been demonstrated in a limited number of cancer-based cell models. In this study, we confirmed that the same axis works in MSCs to modulate cytoskeletal changes that result in enhanced sEV secretion. We observed significant downregulation of RhoA-GTP and p-cofilin in 3D cultured MSCs, which promoted the depolymerisation of F-actin into G-actin, thereby reducing the density of the cortical actin barrier and leading to increased sEV release. However, a missing piece of the puzzle was how MSCs could sense and react to a 3D microenvironment to result in modulation of the Rho/cofilin pathway and downstream effects.

To find the missing link, we looked into the mRNA-seq data and discovered that the identified DEGs for 3D compared to 2D cultured MSCs were enriched in pathways related to integrin-mediated signalling and cytoskeletal metabolism. ITGA1 emerged as a possible candidate, as it is implicated in cytoskeletal dynamics and vesicle regulation (Lindberg et al. 2010; Shi et al. 2012), and was found to be downregulated in our 3D cultured MSCs. Based on the pivotal role of ITGA1 in cell adhesion, migration, and cytoskeletal organisation (Labus et al. 2024), we postulated that it served as the critical link in 3D cultured MSCs, conveying cues from the external culture environment across the membrane surface to modulate the RhoA/cofilin signalling pathway. To test this, we reduced the protein expression level of ITGA1 in MSCs by antibody blocking, which was seen to decrease activation of the RhoA/cofilin signalling pathway as well as cortical actin density, and result in increased sEV secretion. We found an analogous series of events in 3D cultured MSCs, which showed downregulation of membrane-bound ITGA1 together with similar downstream effects. Based on our data, we propose a mechanistic model where MSCs in 3D culture sense the microenvironment through ITGA1, and undergoes cytoskeletal changes by regulating RhoA/cofilin signalling pathway activation. This regulation leads to moderate actin depolymerisation, reducing cortical actin density and thereby lowering barrier resistance to enhance sEV secretion, which works independently from Rab27A/B regulatory pathways.

To accelerate the translation of stem cell-derived EVs into clinical applications for disease treatment, it is necessary to not only solve the problem of upscaling but also to demonstrate improved therapeutic efficacy of EVs arising from new manufacturing processes. We therefore chose two types of possible therapeutic applications of sEVs, OA and wound healing, which both represent highly prevalent diseases with significant unmet needs in clinical treatment. The therapeutic functions of sEVs from 3D cultured MSCs might be particularly relevant to the treatment of these two types of diseases, since the pathogenesis of OA involves



chronic inflammatory responses and dysregulated chondrocyte metabolism (Chen et al. 2022; Pitsillides and Beier 2011), while the progress of skin wound healing can be detrimentally affected by excessive immune responses and fibroblast dysfunction (Peña and Martin 2024). sEVs contain a variety of nucleic acids, with miRNA being a particularly important component of their therapeutic functions from the ability to mediate gene silencing through RNA interference (Isaac et al. 2021). In our 3D culture-derived sEVs, we identified that the top five differentially expressed miRNAs were involved in wound healing, macrophage differentiation, and cartilage development, which could contribute to enhanced therapeutic effects in related disease models. Using in vitro models of chondrocytes and HDFs, we found that sEVs from 3D cultured MSCs significantly promoted cell proliferation and migration while reducing senescence. Moreover, their in vitro immunomodulatory effects were evidenced by promoting macrophage polarisation to the anti-inflammatory M2 phenotype. The anti-inflammatory and pro-regenerative functions of 3D culture-derived sEVs were confirmed in vivo, where treated groups showed more effective protection against OA progression and accelerated skin wound regeneration, highlighting the potential to explore further applications in tissue repair and chronic disease treatment.

In conclusion, this study provided new mechanistic insights into sEV secretion by MSCs in 3D culture. Although Rab27A and Rab27B knockdown in MSCs significantly reduced sEV secretion, their expression levels were similar in MSCs cultured in 2D and 3D environments, and did not explain the elevated sEV secretion seen in 3D cultured MSCs. We elucidated the regulatory pathway governing sEV secretion in 3D culture, which in MSCs is mediated by downregulation of ITGA1, leading to inhibition of the RhoA/cofilin signalling pathway that subsequently increases cortical actin depolymerisation, and enhances sEV release independently of Rab27A/B. Coupled with the superior therapeutic effects of 3D culture-derived sEVs in OA and wound healing models, our study suggests that harnessing these new mechanisms of sEV secretion from MSCs could accelerate the use of sEVs in clinical applications.

## 4 | Methods

All detailed methods are provided in the [Supplementary Information](#). All results presented are from at least three independent experiments for each condition. Data are expressed as mean  $\pm$  standard deviation (S.D.). Statistical comparisons between two independent groups were performed using an unpaired two-tailed *t*-test, while multiple group comparisons were conducted using one-way ANOVA followed by Tukey's post-hoc test. Data from ordinal grading systems were analysed with the nonparametric Kruskal–Wallis test, followed by Dunn's post-hoc test. The sample size (*n*) represents the number of biologically independent samples. Statistical analyses were primarily conducted using GraphPad Prism v8.0, except where otherwise noted, with OriginPro 2021 SR1 (v9.8.0.200) also employed. Exact *p* values are provided in the figures when available; for *p* values smaller than 0.0001, *p* < 0.0001 is reported due to software limitations. Significance was set at *p* < 0.05. Error bars represent the standard deviation for parametric data and the 95% confidence intervals for nonparametric data.

## Author Contributions

**Zhen Yang:** Conceptualization (lead); data curation (lead); formal analysis (equal); methodology (equal); project administration (lead). **Xiaoke Li:** Conceptualization (equal); data curation (equal); formal analysis (equal); methodology (equal); software (lead). **Qiyuan Lin:** Conceptualization (equal); data curation (equal); resources (equal). **Fanfan Zhou:** Project administration (equal); visualization (equal); writing—original draft (equal). **Kaini Liang:** Resources (equal); software (equal); supervision (equal); visualization (equal). **Jiao Jiao Li:** Methodology (equal); visualization (equal); writing—review and editing (equal). **Yudi Niu:** Investigation (equal); software (equal); supervision (equal). **Qingchen Meng:** Supervision (equal); validation (equal); visualization (equal). **Tianyuan Zhao:** Formal analysis (equal); methodology (equal). **Hao Li:** Methodology (equal); validation (equal). **Du Wang:** Methodology (equal); project administration (equal). **Jianjing Lin:** Supervision (equal); validation (equal). **Hui Li:** Resources (equal); supervision (equal). **Bin Wang:** Methodology (supporting). **Wei Liu:** Supervision (equal). **Yanan Du:** Supervision (equal). **Jianhao Lin:** Writing—review and editing (equal). **Dan Xing:** Conceptualization (equal); supervision (equal); writing—review and editing (equal).

## Acknowledgements

This work was funded by grants from Beijing Natural Science Foundation (L222087), Peking University Clinical Scientist Training Program (BMU2024PYJH015, supported by “the Fundamental Research Funds for the Central Universities”), Natural Science Foundation of China (82272538), and Innovation Fund for Outstanding Doctoral Students of Peking University Health Science Center. We appreciate the support and assistance provided by Beijing CytoNiche Biotechnology Co. Ltd in the areas of microcarriers and 3D culture. We thank the Institute of Orthopedics, the First Medical Center, Chinese PLA General Hospital, for their assistance with gait analysis.

## Conflicts of Interest

The authors declare no conflicts of interest.

## Data Availability Statement

The data that support the findings of this study are openly available online.

## References

- Alzahofi, N., T. Welz, C. L. Robinson, et al. 2020. “Rab27a Co-Ordinates Actin-Dependent Transport by Controlling Organelle-Associated Motors and Track Assembly Proteins.” *Nature Communications* 11: 3495.
- Bello-Morales, R., A. J. Crespillo, A. Fraile-Ramos, E. Tabarés, A. Alcina, and J. A. López-Guerrero. 2012. “Role of the Small GTPase Rab27a During Herpes Simplex Virus Infection of Oligodendrocytic Cells.” *BMC Microbiology* 12: 265.
- Bernstein, B. W., and J. R. Bamburg. 2010. “ADF/Cofilin: A Functional Node in Cell Biology.” *Trends in Cell Biology* 20: 187–195.
- Borys, B. S., T. So, J. Colter, et al. 2020. “Optimized Serial Expansion of human Induced Pluripotent Stem Cells Using Low-Density Inoculation to Generate Clinically Relevant Quantities in Vertical-Wheel Bioreactors.” *Stem Cells Translational Medicine* 9: 1036–1052.
- Cao, J., B. Wang, T. Tang, et al. 2020. “Three-Dimensional Culture of MSCs Produces Exosomes With Improved Yield and Enhanced Therapeutic Efficacy for Cisplatin-Induced Acute Kidney Injury.” *Stem Cell Research & Therapy* 11: 206.
- Centeno, E. G. Z., H. Cimarosti, and A. Bithell. 2018. “2D Versus 3D Human Induced Pluripotent Stem Cell-Derived Cultures for Neurodegenerative Disease Modelling.” *Molecular Neurodegeneration* 13: 27.



- Cesarz, Z., and K. Tamama. 2016. "Spheroid Culture of Mesenchymal Stem Cells." *Stem Cells International* 2016: 9176357.
- Chen, P., X. Liu, C. Gu, et al. 2022. "A Plant-Derived Natural Photosynthetic System for Improving Cell Anabolism." *Nature* 612: 546–554.
- Chiang, L., J. Ngo, J. E. Schechter, et al. 2011. "Rab27b Regulates Exocytosis of Secretory Vesicles in Acinar Epithelial Cells From the Lacrimal Gland." *American Journal of Physiology. Cell Physiology* 301: C507–C521.
- Colombo, M., G. Raposo, and C. Théry. 2014. "Biogenesis, Secretion, and Intercellular Interactions of Exosomes and Other Extracellular Vesicles." *Annual Review of Cell and Developmental Biology* 30: 255–289.
- Gowrishankar, K., S. Ghosh, S. Saha, R. C. S. Mayor, and M. Rao. 2012. "Active Remodeling of Cortical Actin Regulates Spatiotemporal Organization of Cell Surface Molecules." *Cell* 149: 1353–1367.
- Guo, D., G. Y. L. Lui, S. L. Lai, et al. 2019. "RAB27A promotes Melanoma Cell Invasion and Metastasis via Regulation of Pro-Invasive Exosomes." *International Journal of Cancer* 144: 3070–3085.
- Han, D., J. Yang, E. Zhang, et al. 2020. "Analysis of Mesenchymal Stem Cell Proteomes In Situ in the Ischemic Heart." *Theranostics* 10: 11324–11338.
- Han, Q.-F., W.-J. Li, K.-S. Hu, et al. 2022. "Exosome Biogenesis: Machinery, Regulation, and Therapeutic Implications in Cancer." *Molecular Cancer* 21: 207.
- Headland, S. E., H. R. Jones, A. S. D'Sa, M. Perretti, and L. V. Norling. 2014. "Cutting-Edge Analysis of Extracellular Microparticles Using ImageStream(X) Imaging Flow Cytometry." *Scientific Reports* 4: 5237.
- Hitsuda, A., R. Dan, A. Urakawa, et al. 2022. "25-Hydroxycholesterol-Induced Cell Death via Activation of ROCK/LIMK/Cofilin Axis in Colorectal Cancer Cell Spheroids." *Journal of Steroid Biochemistry and Molecular Biology* 216: 106037.
- Hutagalung, A. H., and P. J. Novick. 2011. "Role of Rab GTPases in Membrane Traffic and Cell Physiology." *Physiological Reviews* 91: 119–149.
- Isaac, R., F. C. G. Reis, W. Ying, and J. M. Olefsky. 2021. "Exosomes as Mediators of Intercellular Crosstalk in Metabolism." *Cell Metabolism* 33: 1744–1762.
- Jeppesen, D. K., A. M. Fenix, J. L. Franklin, et al. 2019. "Reassessment of Exosome Composition." *Cell* 177: 428–445.e18.
- Jeske, R., C. Liu, L. Duke, et al. 2023. "Upscaling Human Mesenchymal Stromal Cell Production in a Novel Vertical-Wheel Bioreactor Enhances Extracellular Vesicle Secretion and Cargo Profile." *Bioactive Materials* 25: 732–747.
- Jeyaram, A., T. N. Lamichhane, S. Wang, et al. 2020. "Enhanced Loading of Functional miRNA Cargo via pH Gradient Modification of Extracellular Vesicles." *Molecular Therapy* 28: 975–985.
- Kouroupis, D., and D. Correa. 2021. "Increased Mesenchymal Stem Cell Functionalization in Three-Dimensional Manufacturing Settings for Enhanced Therapeutic Applications." *Frontiers in Bioengineering and Biotechnology* 9: 621748.
- Labus, J., K. Tang, P. Henklein, et al. 2024. "The  $\alpha(1)$  Integrin Cytoplasmic Tail Interacts With Phosphoinositides and Interferes With Akt Activation." *Biochimica et Biophysica Acta. Biomembranes* 1866: 184–257.
- Lenzini, S., K. Debnath, J. C. Joshi, et al. 2021. "Cell-Matrix Interactions Regulate Functional Extracellular Vesicle Secretion From Mesenchymal Stromal Cells." *ACS Nano* 15: 17439–17452.
- Li, P., G. Wei, Y. Cao, et al. 2018. "Myosin IIa Is Critical for cAMP-Mediated Endothelial Secretion of von Willebrand Factor." *Blood* 131: 686–698.
- Li, Y., W. Liu, F. Liu, et al. 2014. "Primed 3D Injectable Microniches Enabling Low-Dosage Cell Therapy for Critical Limb Ischemia." *Proceedings of the National Academy of Sciences of the United States of America* 111: 13511–13516.
- Lin, T., L. Zeng, Y. Liu, et al. 2003. "Rho-ROCK-LIMK-Cofilin Pathway Regulates Shear Stress Activation of Sterol Regulatory Element Binding Proteins." *Circulation Research* 92: 1296–1304.
- Lindberg, K., A. Ström, J. G. Lock, J.-Å. Gustafsson, L.-A. Haldosén, and L. A. Helguero. 2010. "Expression of Estrogen Receptor Beta Increases Integrin  $\alpha$ 1 and Integrin  $\beta$ 1 Levels and Enhances Adhesion of Breast Cancer Cells." *Journal of Cellular Physiology* 222: 156–167.
- Liu, C., and C. Su. 2019. "Design Strategies and Application Progress of Therapeutic Exosomes." *Theranostics* 9: 1015–1028.
- Matsui, T., Y. Sakamaki, S. Nakashima, and M. Fukuda. 2022. "Rab39 and Its Effector UACA Regulate Basolateral Exosome Release From Polarized Epithelial Cells." *Cell Reports* 39: 110875.
- Menaceur, C., O. Dusaillly, F. Gosselet, L. Fenart, and J. Saint-Pol. 2023. "Vesicular Trafficking, a Mechanism Controlled by Cascade Activation of Rab Proteins: Focus on Rab27." *Biology* 12: 1530.
- Mitchell, T., A. Lo, M. R. Logan, P. Lacy, and G. Eitzen. 2008. "Primary Granule Exocytosis in Human Neutrophils Is Regulated by Rac-Dependent Actin Remodeling." *American Journal of Physiology. Cell Physiology* 295: C1354–C1365.
- Mo, M., Y. Zhou, S. Li, and Y. Wu. 2018. "Three-Dimensional Culture Reduces Cell Size by Increasing Vesicle Excretion." *Stem Cells (Dayton, Ohio)* 36: 286–292.
- Narumiya, S., M. Tanji, and T. Ishizaki. 2009. "Rho Signaling, ROCK and mDia1, in Transformation, Metastasis and Invasion." *Cancer Metastasis Reviews* 28: 65–76.
- Ostrowski, M., N. B. Carmo, S. Krumeich, et al. 2010. "Rab27a and Rab27b Control Different Steps of the Exosome Secretion Pathway." *Nature Cell Biology* 12: 19–30.
- Papadopoulos, A., G. A. Gomez, S. Martin, et al. 2015. "Activity-Driven Relaxation of the Cortical Actomyosin II Network Synchronizes Munc18-1-Dependent Neurosecretory Vesicle Docking." *Nature Communications* 6: 6297.
- Peña, O. A., and P. Martin. 2024. "Cellular and Molecular Mechanisms of Skin Wound Healing." *Nature Reviews. Molecular Cell Biology* 25: 599–616.
- Pfeffer, S. R. 2010. "Two Rabs for Exosome Release." *Nature Cell Biology* 12: 3–4.
- Pincela Lins, P. M., E. Pirlet, M. Szymonik, A. Bronckaers, and I. Nelissen. 2023. "Manufacture of Extracellular Vesicles Derived From Mesenchymal Stromal Cells." *Trends in Biotechnology* 41: 965–981.
- Pitsillides, A. A., and F. Beier. 2011. "Cartilage Biology in Osteoarthritis—Lessons From Developmental Biology." *Nature Reviews. Rheumatology* 7: 654–663.
- Quast, T., B. Tappertzhofen, C. Schild, et al. 2009. "Cytohesin-1 Controls the Activation of RhoA and Modulates Integrin-Dependent Adhesion and Migration of Dendritic Cells." *Blood* 113: 5801–5810.
- Ridley, A. J. 2001. "Rho Family Proteins: Coordinating Cell Responses." *Trends in Cell Biology* 11: 471–477.
- Ritter, A. T., S. M. Kapnick, S. Murugesan, P. L. Schwartzberg, G. M. Griffiths, and J. Lippincott-Schwartz. 2017. "Cortical Actin Recovery at the Immunological Synapse Leads to Termination of Lytic Granule Secretion in Cytotoxic T Lymphocytes." *Proceedings of the National Academy of Sciences of the United States of America* 114: E6585–e6594.
- Sart, S., A. C. Tsai, Y. Li, and T. Ma. 2014. "Three-Dimensional Aggregates of Mesenchymal Stem Cells: Cellular Mechanisms, Biological Properties, and Applications." *Tissue Engineering. Part B, Reviews* 20: 365–380.
- Schmandke, A., A. Schmandke, and S. M. Strittmatter. 2007. "ROCK and Rho: Biochemistry and Neuronal Functions of Rho-Associated Protein Kinases." *Neuroscientist* 13: 454–469.
- Shi, M., V. Pedchenko, B. H. Greer, et al. 2012. "Enhancing Integrin  $\alpha$ 1 Inserted (I) Domain Affinity to Ligand Potentiates Integrin  $\alpha$ 1 $\beta$ 1-Mediated Down-Regulation of Collagen Synthesis." *Journal of Biological Chemistry* 287: 35139–35152.

- Sinha, S., D. Hoshino, N. H. Hong, et al. 2016. "Cortactin Promotes Exosome Secretion by Controlling Branched Actin Dynamics." *Journal of Cell Biology* 214: 197–213.
- Takai, Y., T. Sasaki, and T. Matozaki. 2001. "Small GTP-Binding Proteins." *Physiological Reviews* 81: 153–208.
- Tan, F., X. Li, Z. Wang, J. Li, K. Shahzad, and J. Zheng. 2024. "Clinical Applications of Stem Cell-Derived Exosomes." *Signal Transduction and Targeted Therapy* 9: 17.
- Trifaró, J. M., S. Gasman, and L. M. Gutiérrez. 2008. "Cytoskeletal Control of Vesicle Transport and Exocytosis in Chromaffin Cells." *Acta Physiologica (Oxford, England)* 192: 165–172.
- Wang, B., W. Liu, J. J. Li, et al. 2022. "A Low Dose Cell Therapy System for Treating Osteoarthritis: In Vivo Study and In Vitro Mechanistic Investigations." *Bioactive Materials* 7: 478–490.
- Wang, W., R. Eddy, and J. Condeelis. 2007. "The Cofilin Pathway in Breast Cancer Invasion and Metastasis." *Nature Reviews. Cancer* 7: 429–440.
- Welsh, J. A., D. C. I. Goberdhan, L. O'driscoll, et al. 2024. "Minimal Information for Studies of Extracellular Vesicles (MISEV2023): From Basic to Advanced Approaches." *Journal of Extracellular Vesicles* 13: e12404.
- Xing, D., W. Liu, J. J. Li, et al. 2020. "Engineering 3D Functional Tissue Constructs Using Self-Assembling Cell-Laden Microniches." *Acta Biomaterialia* 114: 170–182.
- Yan, L., and X. Wu. 2020. "Exosomes Produced From 3D Cultures of Umbilical Cord Mesenchymal Stem Cells in a Hollow-Fiber Bioreactor Show Improved Osteochondral Regeneration Activity." *Cell Biology and Toxicology* 36: 165–178.
- Yu, L., Y. Hou, W. Xie, et al. 2020. "Ligand Diffusion Enables Force-Independent Cell Adhesion via Activating  $\alpha 5 \beta 1$  Integrin and Initiating Rac and RhoA Signaling." *Advanced Materials (Deerfield Beach, Fla.)* 32: e2002566.
- Yuan, X., L. Sun, R. Jeske, et al. 2022. "Engineering Extracellular Vesicles by Three-Dimensional Dynamic Culture of Human Mesenchymal Stem Cells." *Journal of Extracellular Vesicles* 11: e12235.
- Zerial, M., and H. McBride. 2001. "Rab Proteins as Membrane Organizers." *Nature Reviews Molecular Cell Biology* 2: 107–117.
- Zhang, K., and K. Cheng. 2023. "Stem Cell-Derived Exosome Versus Stem Cell Therapy." *Nature Reviews Bioengineering* 1–2.

## Supporting Information

Additional supporting information can be found online in the Supporting Information section.

All data supporting the findings of this study are available from the corresponding author on request. Source data are provided with this paper.